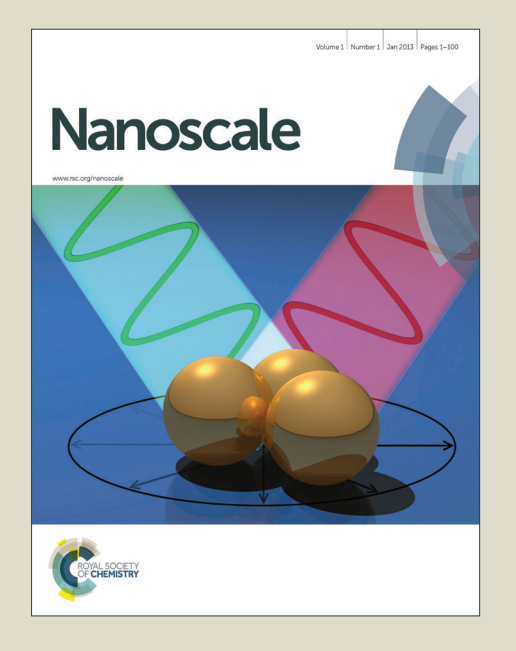
# Nanoscale

Accepted Manuscript



This is an *Accepted Manuscript*, which has been through the Royal Society of Chemistry peer review process and has been accepted for publication.

Accepted Manuscripts are published online shortly after acceptance, before technical editing, formatting and proof reading. Using this free service, authors can make their results available to the community, in citable form, before we publish the edited article. We will replace this Accepted Manuscript with the edited and formatted Advance Article as soon as it is available.

You can find more information about *Accepted Manuscripts* in the **Information for Authors**.

Please note that technical editing may introduce minor changes to the text and/or graphics, which may alter content. The journal's standard <u>Terms & Conditions</u> and the <u>Ethical guidelines</u> still apply. In no event shall the Royal Society of Chemistry be held responsible for any errors or omissions in this *Accepted Manuscript* or any consequences arising from the use of any information it contains.



Combined chemo- and photothermal therapy delivered by multifunctional theranostic gold nanorod-loaded microcapsules

Haiyan Chen<sup>a, §</sup>, Yingfeng Di<sup>a, §</sup>, Dan Chen<sup>a, §</sup>, Kyle Madrid <sup>b</sup>, Min Zhang<sup>a</sup>, Caiping Tian<sup>a</sup>, Liping Tang<sup>c</sup>, Yueqing Gu<sup>a,\*</sup>

<sup>a</sup> Department of Biomedical Engineering, School of Engineering, China

Pharmaceutical University, 24 Tongjia Xiang, Gulou District, Nanjing 210009, China

<sup>b</sup> Department of Chemistry, University of California, Riverside 92507, USA

<sup>c</sup> Department of Bioengineering, University of Texas at Arlington, 701 South

Nedderman Drive, Arlington, TX, 76019, USA

§ Haiyan Chen, Yinfeng Di and Dan Chen contributed equally to the work.

\*Author to whom correspondence should be addressed:

Yueqing Gu, PhD

Email: guyueqing@hotmail.com

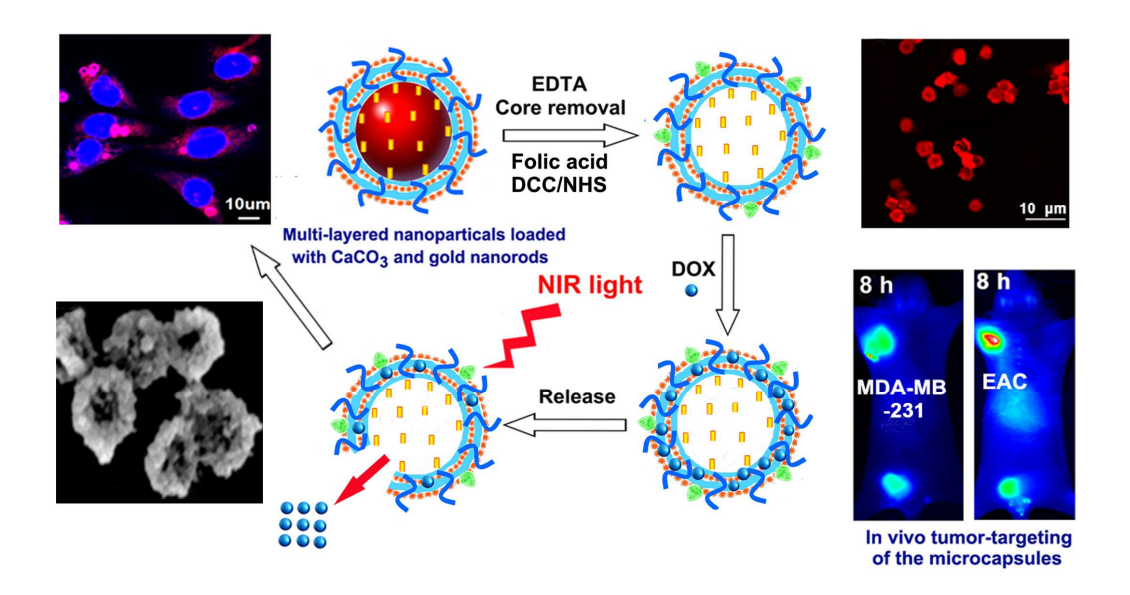
Tel: +86-25-83271080

Fax: +86-25-83271046

# **Abstract**

A polyelectrolyte microcapsule-based, cancer-targeting, and controlled drug delivery system has been developed as a multifunctional theranostic agent for synergistic cancer treatment. This new system, called FA-MC@GNR, is composed of folic acid (FA)-modified, multi-layered, hollow microcapsules loaded with gold nanorods (GNRs), and undergoes thermal degradation under near infrared (NIR) light. Either an NIR dye (MPA) or anti-cancer drug (doxorubicin, DOX) was loaded into the microcapsules via physical adsorption, yielding FA-MC@GNRs/MPA FA-MC@GNRs/DOX, both exhibiting no obvious toxicity, high stability, and remarkably improved tumor-targeting capabilities in vivo. Utilizing the strong NIR absorption of FA-MC@GNRs/DOX, we demonstrate the system's ability to simultaneously elicit photothermal therapy and controlled chemo-therapy, achieving synergistic cancer treatment both in vitro cellular and in vivo animal experiments. Our study presents a new type of multifunctional micro-carrier for the delivery of chemo-therapeutic drugs and photothermal agents, which has been shown to be an effective therapeutic approach for combined cancer treatment.

**Keywords:** multi-functional microcapsule, gold nanorods, near infrared irradiation, tumor-targeting, in vivo imaging, combined therapy



**Graphical Abstract:** Synthesis and characterization of the multifunctional theranostic microcapsules for combined chemotherapy and photothermal therapy.

# 1. Introduction

There has been a growing interest in the design and development of polyelectrolyte microcapsules as controlled drug delivery systems.<sup>1,2</sup> In particular, hollow polyelectrolyte microcapsules assembled via the layer-by-layer (LbL) technique<sup>3-5</sup> have attracted much attention for drug delivery because of their unique properties, including large drug-loading capacity, mild synthesis conditions, controllable surface properties, and responsiveness to various environmental stimuli.<sup>6-8</sup> Hollow polyelectrolyte microcapsules are produced by the sequential adsorption of oppositely charged molecules, such as polyelectrolytes, onto charged sacrificial template-particle seeds,<sup>9,10</sup> which are later dissolved, resulting in hollow cavities for drug encapsulation. These microcapsules can be readily produced at room temperature using electrostaticadsorption without organic solvents or harsh reaction conditions. Additionally, the physicochemical properties of the microcapsule shells can be precisely tuned and the surface can be decorated with a wide variety of functional molecules, such as folic acid<sup>11</sup>, polyethyleneglycol<sup>12</sup> or antibodies.<sup>13</sup>

Recently, studies have shown a synergistic anti-tumor effect when chemotherapy and thermotherapy are combined in nanomedicine. <sup>14, 15</sup> This study aimed to develop a new group of polyelectrolyte microcapsules with the capability to target tumors and elicit localized thermal and chemotherapeutic effects. Until now, only a few works have been reported regarding polyelectrolyte microcapsule applications in animal experiments. Currently, the main challenge in microcapsule design is ensuring direct delivery of the chemotherapy drug to cancerous tissues without causing systemic side

effects in vivo. Zhao et al. reported an anti-tumor study involving direct intratumoral injection of Doxorubicin (DOX)-loaded microcapsules.  $^{16}$  Shen et al. demonstrated that capsules with an average diameter of  $5.4 \pm 0.9$  µm were entrapped in the pulmonary circulation after intravenous injection.  $^{17}$  De Koker and coworkers reported the in vivo consequences of subcutaneous polyelectrolyte microcapsule injection, including microcapsule fate as well as tissue and immune responses.  $^{18}$ 

Gold nanorods (GNRs), an excellent photo-thermal agent through plasmon-assisted processes, have recently attracted much interest as potential vehicles for treating cancer via thermal-therapy. <sup>19, 20</sup> This is achieved by tuning the light absorption of the GNRs to the near infrared (NIR) range, which is characterized by deep tissue penetration and a high photo-thermal effect. Notable benefits of using GNRs are the advantages of large-scale synthesis, easy functionalization, and colloidal stability. <sup>21, 22</sup>

In the present study, Dovorubicin (DOX), a widely used clinical anti-cancer drug.

In the present study, Doxorubicin (DOX), a widely used clinical anti-cancer drug, was immobilized within microcapsule cavities to form a nano-drug known as MC@GNRs/DOX. Folate (FA) was covalently attached onto the MC@GNRs/DOX surface to form FA-MC@GNRs/DOX, a tumor-selective micro-conjugate that holds potential in optical imaging due to its ability to specifically target over-expressed FA receptors in malignant cells. The photo-thermal effect as well as the release behavior of FA-MC@GNRs/DOX was evaluated and the combined chemo-photothermal therapeutic efficacy after intratumoral and intravenous injection was also compared in tumor-bearing mice.

# 2. Experimental

#### 2.1 Materials

Ca(NO<sub>3</sub>)<sub>2</sub>.4H<sub>2</sub>O, NaCO<sub>3</sub>, AgNO<sub>3</sub>, Ethylene Diamine Tetra-acetic Acid (EDTA), Sodium borohydride (NaBH<sub>4</sub>), absoluteethylalcohol, uranine, chloroauric acid (HAuCl<sub>4</sub>), cetyltrimethylammoniumbromide (CTAB), ascorbicacid (AA)were all purchased from China National Medicine Corporation Ltd., and glutaraldehyde (GA) was purchased from Shanghai Wulian chemical. Sodiumpolystyrenesulfonate (PSS), Chitosan (CS), and Sodium alginate (SA) were purchased from Sigma-Aldrich and used as starting materials without further purification.

MPA (MW: 995) was prepared in our laboratory. DOX (MW: 149.15); FA; 1-ethyl-3-[3-dimethylaminopropyl] carbodiimide hydrochloride (EDC); N, N'-Dicyclohexylcarbodiimide (DCC); and N-hydroxysuccinimide (NHS) were purchased from Sigma-Aldrich. 3-(4,5-dimethylthi-alzol-2-yl)-2, 5-diphe-nyltetrazolium bromide (MTT) and fetal bovine serum (FBS) were all purchased from HyClone. All other solvents and reagents used in this study were certified analytical reagent grade.

## 2.2 Synthesis of MC@GNRs, MC@GNRs/DOX and FA-MC@GNRs/DOX

Gold nanorods (GNRs) were prepared by an improved seed-mediated method.<sup>23</sup> The seed solution was prepared by rapidly adding ice cold NaBH<sub>4</sub> solution (0.1 M, 0.6 mL) into a mixture containing 5 mL of HAuCl<sub>4</sub> (0.0005 M) and 5 mL of CTAB (0.2 M), followed by vigorous stirring for 1 min. Then, 0.24 mL of seed solution was injected into a growth solution containing CTAB (100.0 mL, 0.1 M), HAuCl<sub>4</sub> (100.0 mL, 0.1 M), AgNO<sub>3</sub> (5.0 mL, 10.0 mM) and ascorbic acid (1.4 mL, 0.0788 M).

As-grown GNRs were further subjected to overgrowth, and GNRs with an enhanced absorption peak around 765 nm were obtained. After 1 h, the reaction was stopped by centrifugation (12 000 rpm, 10 min). The precipitates were then collected and re-dispersed in deionized water.

MC@GNRs was prepared by using calcium carbonate (CaCO<sub>3</sub>) microparticles as a sacrificial template. CaCO<sub>3</sub> microparticles were synthesized according to Volodkin's work.<sup>24</sup> In detail, GNRs, PSS solution, Ca(NO<sub>3</sub>)<sub>2</sub> and Na<sub>2</sub>CO<sub>3</sub> solutions (0.025 M) were mixed with vigorous stirring and sonicated for 15 s, followed by extensive washing with pure water to remove un-reacted reagents. Finally, GNR-loaded CaCO<sub>3</sub> (GNR/CaCO<sub>3</sub>) core templates were obtained.

The GNR/CaCO<sub>3</sub> cores were coated with chitosan and sodium alginate via the layer-by-layer (LbL) technique. The cores were dispersed in 1 mL of water with 200 μL of chitosan solution (2 mg/mL). After vigorously stirring for 15 min, the microparticles were collected by centrifugation, and residual chitosan was removed by washing twice with pure water. Thereafter, the microparticles were suspended in water (1 mL) with sodium alginate solution (200 μL) and shaken for 15 min, followed by centrifugation and two washing steps. This procedure was repeated to generate up to different numbers of layers (5 to 13). After addition of 1.0 mL of glutaraldehyde (GA) aqueous solution (25 wt %), the system was stirred at 300 rpm for 30 min to yield the microparticles covered with cross-linked layers. Hollow microcapsules loaded with GNRs (MC@GNRs) were obtained by the removal of the CaCO<sub>3</sub> core via incubation with 0.2 M EDTA solution for 30 min at room temperature, followed by

multiple washes with pure water.

FA was covalently conjugated to MC@GNRs to form FA-MC@GNRs.<sup>25</sup> First, FA was reacted with DCC/NHS (molar ratio of FA: DCC: NHS is 1: 1.5: 2) in anhydrous dimethyl sulfoxide (DMSO, 2.5 mL) and the mixture was stirred in the dark for 12h at 50 °C. The residue was removed by filtration under reduced pressure and centrifugation (16000 rpm) for 10 minutes, and the activated FA was extracted by adding 10 mL anhydrous acetone. After dissolving the activated FA in Tris buffer (1 mL, 10 mM, pH 8.0), the resulting solution was mixed with MC@GNRs in Tris buffer and stirred in the dark for 12 h at 4 °C. The obtained products were followed by multiple washes with pure water to obtain FA-MC@GNRs.

For DOX loading, DOX (1.0 mg) was added into FA-MC@GNRs solution (10.0 mL, 100 μg mL<sup>-1</sup>) and then stirred for 24 h at 37 °C. During the incubation, DOX was self-absorbed into the multi-layers of FA-MC@GNRs by electrostatic interaction. Subsequently, DOX loaded FA-MC@GNRs (FA-MC@GNRs/DOX) were washed by centrifugation (4500 rpm, 5 min) and re-suspended in Millipore water. This process was repeated four times. The NIR fluorescent dye MPA was also loaded into FA-MC@GNRs to form FA-MC@GNRs/MPA for *in vivo* imaging following the method described above.

The DOX and GNRs loading was all calculated according to the formula: drug loading (DL) = (mass of drug loaded in the microcapsules / total mass of drug loaded and the microcapsules).

# 2.3 Characterization

The size and morphology of GNRs and FA-MC@GNRs were measured by a JEM-2000 EX II transmission scanning electron microscope (TEM, JEOL Company, USA) and a JSM-7500F scanning electron microscope (SEM, JEOL Company, USA) and the fluorescence images of FA-MC@GNRs/DOX were acquired by a FV1000 laser confocal fluorescence microscope (LCFM, Olympus, Japan). The hydrodynamic size and zeta-potential of the microcapsules were measured by Zetasizer (Brookhaven Instruments Corporation, USA) at a temperature of 25 °C. The absorption spectra of the microcapsules were acquired by a Lambda 25 UV-Vis spectrophotometer (Perkin Elmer, USA).

The release of GNRs and DOX from the microcapsules was investigated. FA-MC@GNRs/DOX solution was placed in a dialysis bag (cellulose ester, MWCO of 300 kDa). The dialysis bag was immersed in 50 mL of phosphate-buffered saline (PBS) containing 10 % fetal bovine serum (FBS) in a shaking rocker at 100 rpm and maintained at 25 °C or 37 °C for 48 h. The amount of drug released over time was recorded using a UV spectrophotometer, and the concentration was calculated from a standard calibration curve.

The photo-thermal effect of FA-MC@GNRs was determined by measuring the mixture temperature at different NIR irradiation times. PBS, MC, GNRs, and FA-MC@GNRs in DMEM (50  $\mu$ g/mL) were added separately into a 96-well plate. The resulting temperature increase in each well was monitored during 30 min exposures to a 765 nm laser (nLight, Shanghai Optics Company). The beam diameter was 1 cm and the power density of the laser source was fixed at 1.0 W/cm<sup>2</sup>.

Additionally, the photo-thermal effect on the microcapsule morphology was also assessed by SEM. The drug-releasing profile for FA-MC@GNRs/DOX was obtained by subjecting the sample to NIR light irradiation for 30 min, centrifuging at 5000 rpm for 10 min, and determining the concentration of DOX in the supernatant by measuring its UV-vis absorption at 485 nm.

Additionally, the controlled release capability of FA-MC@GNRs/DOX was observed *in vitro* using three tumor cell lines (MDA-MB-231, MCF-7 and U87). Briefly, the cells were seeded in LCFM culture dishes with a density of  $1\times10^5$  cells/well and incubated at 37 °C. When the whole cells reached 70 % ~ 80 % confluence, 100  $\mu$ L of FA-MC@GNRs/DOX (50  $\mu$ g/mL) was added to the dishes, which were then incubated for 12 h followed by incubation with Hoechst 33342 solutions (100  $\mu$ L, 10  $\mu$ g/mL) for 30 min. After completely washing with DMEM media to remove any free microcapsules, the cells in the culture dish were subjected to NIR irradiation, and the cells were then examined by LCFM at 30 min and 2 h after irradiation respectively. In addition, a typical series of images before and after NIR irradiation was acquired.

#### 2.4 *In vitro* cytotoxicity assay

The cell morphology and viability were used to assess the cytotoxicity of the microcapsules *in vitro*. Different tumor cells were plated at a density of  $4 \times 10^5$  cells/dish in a confocal-specific dish and subsequently cultured for 24 h. The cells were incubated with 100  $\mu$ L of PBS, DOX, GNRs (laser), FA-MC@GNRs/DOX and FA-MC@GNRs/DOX (+ laser) respectively for 12 h. The laser (765 nm) with 2.0 cm

beam diameter and 1.0 W/cm² power density was utilized to irradiate the cell dishes for 20 min. The residual cells and the morphological changes were displayed by the differential interference contrast (DIC) mode of LCFM. The therapeutic effect of various samples on MDA-MB-231 cells and HBL-100 was also evaluated using an MTT assay. The cells were exposed to the 765 nm laser for 20 min, and then incubated for another 12 h. Cell viability was calculated based on the following formula: Cell viability = (Mean absorbance of test wells - Mean absorbance of medium control wells) / (Mean absorbance of untreated wells - Mean absorbance of medium control well) × 100 %.

# 2.5 Acute toxicity evaluated in mice

Athymic nude mice and normal (Kunming) mice were purchased from Charles River Laboratories (Shanghai, China) for investigation via in vivo imaging. All animal experiments were carried out in compliance with the Animal Management Rules of the Ministry of Health of the People's Republic of China (Document NO. 55, 2001) and the guidelines for the Care and Use of Laboratory Animals of China Pharmaceutical University.

To evaluate acute toxicity of FA-MC@GNRs/DOX, the healthy Kunming mice (15 male and 15 female) were randomly assigned into three groups (saline, DOX or FA-MC@GNRs/DOX). The above samples (0.2 mL) were injected through the tail vein into the irrespective group. Blood was then drawn from the eye socket 7 days post-injection. Serum biochemical parameters including aspartateamino transferase (AST), alanine aminotransferase (ALT), blood urea nitrogen (BUN) and creatine

kinase (CK) indexes of the blood samples were examined.

2.6 Dynamics and targeting ability of FA-MC@GNRs/MPA in tumor-bearing mice

To investigate the tumor affinity of the probes, athymic nude mice (n = 15) were separated randomly into three groups and subcutaneously injected with either MDA-MB-231 cells, MCF-7 cells, or Ehrlich Ascites Carcinoma (EAC) cells ( $\sim 5 \times 10^6$  in 50  $\mu$ L of PBS) in the axillary fossa.

Normal mice were first injected with FA-MC@GNRs/MPA and free MPA in the tail vein. The resulting dynamic distribution of the two probes was monitored by NIR imaging at different times within 48 h post-injection. Background images were also obtained for each mouse prior to injection.

FA-MC@GNRs/MPA was intravenously injected into the cell lines with different folate receptor (FR) expression levels: MDA-MB-231 (high FR level), MCF-7 (low FR level), and EAC (high FR level) tumor-bearing nude mice and monitored by NIR fluorescence imaging for up to 48 h post-injection. To assess the tumor-targeting specificity of the microcapsules, tumor-to-normal tissue contrast ratios (T/N) at different times were calculated by using ROI functions with Scion Image software. To further investigate the bio-distribution of the microcapsules in living mice, the major organs (heart, liver, spleen, lung, kidney, and intestine) as well as the tumor of the subjected MDA-MB-231 mice were excised at 48 h post-injection and detected by NIR fluorescence imaging.

#### 2.7 Anti-tumor efficacy evaluation

EAC tumor-bearing (0.5 cm) mice were randomly assigned into six groups (n = 6).

200  $\mu$ L of saline, DOX (5 mg / kg), GNRs, or FA-MC@GNRs/DOX (containing 5.0 mg/kg DOX) were intratumoral injected and FA-MC@GNRs/DOX (containing 5.0 mg/kg DOX) was also intravenously administered to the mice. The FA-MC@GNRs/DOX groups and GNR group were exposed to 1.0 W/cm² NIR light for 15 min at 8 h post-injection. Subsequently, each mouse underwent repeated tail vein injections once every other day. The tumor volume and body weight of each mouse were monitored every three days for 15 days. The tumor volume was calculated as length× (width)² × 1/2. The survival rate of the treated mice was calculated according to the equation: Survival rate = Ns/Nt × 100 %, where Ns and Nt represent the number of surviving mice and the number of total mice in each group respectively.

#### 2.8 Histological analysis

To further investigate the therapeutic effects of intratumoral injection of FA-MC@GNRs/DOX in EAC tumor-bearing mice, the tumors were excised for histo-pathologic analysis 15 days post-injection. The tissue was fixed with 10 % neutral buffered formalin and embedded in paraffin. The tumors (8 mm) cross-sections were stained with Hematoxylin and Eosin (H&E) and observed with a BX41 bright field microscope (Olympus).

# 3. Result and Discussion

### 3.1 Synthesis and characterization of the microcapsules

The microcapsules (FA-MC@GNRs/DOX) were synthesized according to the routine illustrated in Figure 1. GNRs mixed with PSS were used to form the

GNR-loaded core template of the microcapsules. A GNRs@CaCO<sub>3</sub> core template (negatively charged) was coated with 9 layers of alternating positively charged chitosan and negatively charged sodium alginate and the core was removed with EDTA. FA was conjugated on the surface of the microcapsule and DOX was then loaded into the core.

The layer coating process was monitored by measuring zeta potential variation. As shown in Figure 2A, the diameters of the microcapsules coated with 9-layer biocompatible polyelectrolyte were about  $2.6 \pm 0.4 \, \mu m$  (polydispersity index: 0.295). The diameter of the microparticles was determined by the size of CaCO<sub>3</sub> core and did not change after the coating layers were applied. Successful coatings were assessed by the alternating positive and negative charge potential variations present on the capsule surface. As shown in Figure 2B, starting from a GNRs@CaCO<sub>3</sub> microparticle with a zeta-potential of -14.5 mV, the zeta-potential alternated between -22.8 mV and 33.5 mV during the deposition of 9 polyelectrolyte layers. These results demonstrate the successful synthesis of a microcapsule coated with alternating layers of chitosan and sodium alginate.

For the thermal therapy application, GNRs were loaded into the core of the microcapsules. The GNR length was approximately  $15 \pm 1.32$  nm and the average aspect ratio (length/diameter) was  $4.2 \pm 0.4$  (Figure 3A). The SEM image reveals the concave shape of the microcapsules. The cores of FA-MC@GNRs/DOX microcapsules are dark, indicating the cavity appeared inside the microcapsules. We further conclude from the TEM image inserted in Figure 3B that GNRs are densely

loaded inside the microcapsules. Furthermore, the LCFM image (Figure 3C) displays the bright red fluorescence of DOX, which confirms its loading into the FA-MC@GNRs microcapsules.

The successful loading of GNRs and DOX in the interior of microcapsules was further demonstrated by the absorption and fluorescence spectra. The aspect ratio (length/diameter  $4.2 \pm 0.4$ ) of the nanorods results in an average longitudinal surface plasmon resonance wavelength of 765 nm and a weak transverse plasmon band at 510 nm, which is clearly indicated in Figure 4A. There were no obvious differences between the absorption wavelengths of GNR-loaded microcapsules and free GNRs. In the presence of 10% FBS solution at room temperature (25°C), less than 7 % of loaded DOX was released from the microcapsules (FA-MC@GNRs/DOX) within 48 h of incubation (Figure 4B). Moreover, less than 10 % of loaded DOX was released at 37 °C. This slow leakage indicates that the drug-loaded microcapsules may reduce the toxicity and side effects of chemotherapeutic drugs by preferentially delivering them to target tissues.

3.2 Drug loading capacity, drug release behavior and photo-thermal properties of the microcapsule system

The thickness of the layers is the key factor to determine the loading capacity of DOX and GNRs. In this study, the thickness of the layers was investigated to determine its influence on the loading capacity of the drugs. Figure 5A exhibits the variation of the drug (DOX/GNRs) loading capacity as a function of the number of polyelectrolyte layers. The loading capacity of DOX is 9.8±0.6% and the loading

capacity of GNRs was 8.7±0.8% when nine layers are coated on the surface of the microcapsules. The loading capacity of DOX or GNRs decreases accordingly when the layer numbers deviate from 9. It suggests that nine layers is preferred to be selected for the synthesis of microcapsules.

As GNRs possess high absorption coefficients, the GNR-loaded microcapsules showed strong absorption at 765 nm and consequently converted the absorbed light into heat,<sup>27</sup> resulting in increased surrounding temperatures. As shown in Figure 5B, the temperature of the GNRs and MC@GNRs increased during the initial period and gradually reached a plateau within 30 min of irradiation with a 765 nm laser. In contrary, no temperature change was detected for PBS and MC under NIR light irradiation. Next, the effect of NIR irradiation on the microcapsule morphology was observed using SEM. Similar to a concave and a convex on a deflated ball, the shape of the microcapsules depends on the view angles. As indicated in Figure 5C, FA-MC@GNRs/DOX displays no obvious morphology changes after 5 min of NIR irradiation. The morphology changes of the typical microcapsule are shown on the bottom panel, indicating their gradual collapse after 10 min of NIR light irradiation. After 20 min, the majority of the microcapsules broken open and fragmented. Further exposure resulted in the disruption of the polyelectrolyte network and the disintegration of the shell.

DOX, an antitumor drug, was selected as a model substance to be encapsulated in the GNR-loaded microcapsules to form FA-MC@GNRs/DOX. The loading capacity of doxorubicin in the microcapsules was  $10.56 \pm 0.48 \%$  (w/w). As illustrated in

Figure 5D, the release of DOX elevated in response to irradiation time, and plateaued at about 30 min equating to 80 % of loaded DOX liberated. Meanwhile, the temperature profile increase behaved similarly, characterized by a quick initial elevation and a plateau at about 20 min of irradiation exposure. The photo-thermal effect of the GNR induces the temperature increase and leads to the collapse of the microcapsules after NIR irradiation, which also indicates DOX release. These results imply that an irradiation period of 20-30 min is adequate for capsule fracture and subsequent DOX/drug release. Interestingly, 100 % DOX releasing could not attained even after prolonged NIR irradiation, which might be attributed to entrapment within the polyelectrolyte matrix. To increase the stability of the polyelectrolyte coated on the surface of GNRs via LbL technique, GA was introduced for cross-linking of the multi-layers. GA is not stable in high temperature. As the GNRs loaded in the cores of the FA-MC@GNRs was irradiated by the NIR light, the temperature in the cores of the microcapsules increased obviously, which resulted in the degradation of the aldehyde groups of GA. Thus, the multi-layers became unstable and degraded, and the entrapped DOX was released.

The results of controlled DOX release from FA-MC@GNRs/DOX at the cellular level are shown in Figure 6. After 12 h of incubation, the DOX-loaded microcapsules were attached to MDA-MB-231, MCF-7 and U87 tumor cells. After exposure to NIR light irradiation for 30 min, the red fluorescence was observed to spread over the cytosol. The red fluorescence appeared evidently at the cytoplasm and cell nuclear at 2 h after irradiation, which suggested that the microcapsules are internalized instead

of attaching on the cell membranes. These results further validate that the release of DOX from FA-MC@GNRs/DOX can be controlled by NIR light.

# 3.3 *In vitro* cytotoxicity of FA-MC@GNRs/DOX

The cytotoxicity of our MC@GNRs-based drug delivery system was investigated in three different tumor cell lines (MDA-MB-231, MCF-7 and U87). As shown in Figure 7A, each group showed different degrees of morphology changes. The majority of cells groups incubated with saline, NIR light, and FA-MC@GNRs/DOX without irradiation maintained their original spindle-shaped morphology, indicating the low cytotoxicity of these samples. On the other hand, as expected, cells incubated with free DOX and FA-MC@GNRs/DOX+laser exhibited obvious morphological changes with abundant round and non-adherent cells. It is worth noting that the GNRs+laser treated group displayed partial cell morphology changes, indicating the efficacy of GNR-mediated thermal therapy. Furthermore, a quantitative evaluation of cytotoxicity was carried out in both cancer cells and normal cells by an MTT assay (Figure 7B and Figure 7C). Cells treated with laser irradiation or FA-MC@GNRs/DOX exhibited high cell viability, also implying the low cytotoxicity of these two treatments. Other groups treated with DOX, GNRs+laser, and FA-MC@GNRs/DOX+laser exhibited dose-dependent anti-tumor activity. In particular, FA-MC@GNRs/DOX+laser showed the highest cytotoxicity; at the highest dose level, this treatment group demonstrated a cell inhibition ratio larger than 90 %, which was much higher than groups treated with GNRs+laser (60 %) and DOX (74 %). This high therapeutic efficacy can be attributed to the microcapsules' combined thermal therapy and chemotherapy actions. These treatments exhibited a similar level of cytotoxicity on normal breast cells (HBL-100), demonstrating the independence of their effects on cell type.

3.4 *In vivo* dynamic distribution in normal mice and tumor-targeting ability of FA-MC@GNRs/MPA in tumor bearing mice

The safe circulation of microparticles in the blood vasculature of mice has a significant impact on the development of drug carriers at the micron level. <sup>28-30</sup> The NIR fluorescence dye (MPA) was loaded into the microcapsules (FA-MC@GNRs) to form FA-MC@GNRs/MPA for tracking the biodistribution of the microcapsules, generating a series of NIR fluorescence images at different times (Figure 8A). FA-MC@GNRs/MPA were distributed throughout the body within 2 h post-injection, concentrated in liver after 4h, and gradually expelled after 48 h. Although most of the microcapsules were removed through the intestines, accumulation in liver at 48h was still detectable. In contrast, MPA rapidly spread through the body and was near completely filtered out by the kidneys after 8 h post-injection (Figure 8B). Ultimately, the accumulation of MPA in the main metabolic tissues (liver, kidney) was negligible after 48 h post-injection. The differences in the dynamic distribution of FA-MC@GNRs/MPA and MPA illustrate the microcapsule's influence on the biodistribution of the dye and its role in extending MPA's circulation lifetime in the body. Additionally, the delayed clearance of in vivo fluorescent signals from the FA-MC@GNRs/MPA-treated group implies the successful entrapment of MPA in the microcapsules.

To ascertain the biodistribution of the microcapsule system, a cohort of mice were euthanized and the main organs were excised for *ex vivo* fluorescence imaging at 24 h post-injection. As shown in Figure 8C, the microcapsules were mostly distributed in the liver and intestine, while a lower concentration appeared in the heart, spleen, lung and kidney. These *ex vivo* imaging results are consistent with those of the *in vivo* imaging. For semi-quantifying the distribution of the microcapsules in the main organs, the contrast ratios were analyzed (Figure 8D). Intense fluorescence was observed in the liver and intestine 4 h post-injection, which gradually faded after 8 h. No obvious fluorescence appeared in the heart, spleen or lung.

Fluorescence imaging performed after microcapsule injection via tail vein did not reveal any vascular blockage. In addition, mice treated with FA-MC@GNRs/MPA did not exhibit any unhealthy symptoms and maintained the same lifetime as mice in the control group. Furthermore, no animal fatality resulted from daily intravenous microcapsule injections (DOX concentration of 16.5 mg/kg) for 7 days. The acute toxicity of the microcapsules was examined based on biochemical parameters, including ALT, AST, BUN, and CK (Figure 9A). ALT (liver), AST (liver), BUN (kidney), and CK (heart) levels in mice administrated with microcapsules were much lower than those treated with an equivalent amount of free DOX. No significant differences in ALT, AST, BUN, and CK were observed between the microcapsule (FA-MC@GNRs/DOX) group and the saline group, indicating that the encapsulation of DOX significantly reduces its heart and liver toxicity. Examination of the H&E-stained major organ, tissue (heart, liver and kidney) cross sections (Figure 9B)

suggests that animals treated with FA-MC@GNRs/DOX do not experience any toxic effects within 7 days post-treatment. These results suggest the low bio-toxicity of the microcapsules *in vivo*.

In order for nanoparticles-based treatments to be viable, it is critical that the injected particles can preferentially accumulate at desired sites and then be subsequently evacuated from the body. To target cancerous cells, FA was conjugated on the microcapsule shell to form FA-MC@GNRs/MPA. Mice bearing an MDA-MB-231 tumor (high FR level) and an MCF-7 tumor (low FR level) were administrated FA-MC@GNRs/MPA and imaged at different times (Figure 10). Significant uptake of FA-MC@GNRs/MPA in the tumor was clearly visible in MDA-MB-231 mice at 4 h post-injection. The maximum fluorescence signal in the tumor appeared at 12 h post-injection, and the high tumor to muscle contrast persisted for more than 48h (Figure 10A). In comparison, the MCF-7 tumor's fluorescence signal was detectable 8h after injection of the probe and rapidly disappeared within 24 h, which can be attributed to the enhanced permeation and retention effect (Figure 10B). The ex vivo fluorescence images of the excised organs from MDA-MB-231 tumor-bearing mice at 48h post-injection confirm the high tumor specificity of FA-MC@GNRs/MPA (Figure 10C). The tumor-to-normal tissue ratios of the MDA-MB-231 mice were distinctly higher than that of the MCF-7 tumor-bearing mice (Figure 10D). The in vivo fluorescence imaging results indicate that FA-conjugated microcapsules could serve as an ideal drug carrier due to their selective accumulation in tumors with high folate receptor expression.

Furthermore, the tumor-targeting ability of FA-conjugated microcapsules was assessed in EAC (high FR level) tumor-bearing mice via both intratumoral and intravenous injection. As shown in Figure 11A, FA-MC@GNRs/MPA, when intratumoral injected, was entrapped in the tumor over the entire experimental period (48 h). The *ex vivo* NIR imaging of isolated organs confirmed this *in vivo* observation. The intravenously injected microcapsules also demonstrated active tumor-targeting ability (Figure 11B). All of these results indicate that FA-MC@GNRs/MPA could act as an effective drug carrier for FA positive tumor-targeting delivery through either intratumoral or intravenous administration.

# 3.5 Therapeutic efficacy of FA-MC@GNRs/DOX in tumor-bearing mice

In order to quantitatively analyze the effectiveness of different treatments, the tumor volume, survival rate, and body weight of each group of mice were recorded at different times (Figure 12). As illustrated in Figure 12A, mice treated with FA-MC@GNRs/DOX without laser irradiation had fates similar to those treated with saline. No obvious therapeutic effects were observed in FA-MC@GNRs/DOX-treated mice, implying that very little DOX leaked from the microcapsules. Mice treated with GNRs+NIR laser irradiation exhibited obvious benefits (versus mice treated with saline), which could be attributed to thermal therapy. The mice treated with free DOX showed favorable anti-tumor chemotherapy activity. In comparison, mice injected with FA-MC@GNRs/DOX+laser displayed more effective tumor inhibition than any other treatment, illustrating the combined effects of thermal therapy and chemotherapy. In addition, the therapeutic results observed in the intratumoral

injected group were similar to those of the intravenously injected group. As shown in Figure 12B, the body weight of mice in the FA-MC@GNRs/DOX (without irradiation) and control groups began to decrease from day 9 post-injection, indicating that the mice's living quality was compromised by the tumor burden. Mice survival rates in the control, DOX, and microcapsule groups without light irradiation were 33.7 %, 66.6 %, and 50.0 % respectively, at day 15 (Figure 12C). There were no deaths among mice treated with FA-MC@GNR/DOX+laser. These results demonstrate that combined therapy based on FA-MC@GNR/DOX can effectively improve the survivorship of mice and extend their lifetime. Pathohistological analysis (Figure 12D) of tissue from different treatment groups reveals that no observable damage took place in the tumors of control mice 7 days post-treatment. While GNR and DOX groups had a lower level of tumor tissue destruction, significant apoptosis occurred in the peripheral and central tumor region for the FA-MC@GNRs/DOX+laser group, resulting in only a small amount of living tumor cells around the tumor vessels.

Both of the two FA-MC@GNRs/DOX administrations led to similar therapeutic outcomes, including survival rate, tumor volume, and body weight. Commonly, intratumoral injection, which relies on enhanced retention and permeation, delivers a higher concentration of the multifunctional microcapsules to the tumor than intravenous injection. In this study, the intratumor treatment group was intratumor-injected only on the first injection. The more obvious differences are expected to be observed if FA-MC@GNRs/DOX was injected intratumoral in all the therapy period.

The photothermal effect of gold nanoparticles such as nanorods, nanocages (NCs), nanoshells and nanoflowers, has been widely exploited for the photothermal ablation of tumor cells. It is desirable to facilitate the gold nanoparticles to generate high temperatures at desired sites other than the whole-body. Dickerson and his co-workers designed gold nanorods that can be directed to the squamous cell carcinoma in mice. leading to the selective localization of hyperthermic treatment.<sup>31</sup> Li et al. demonstrated in vivo tumor targeting and photothermal therapy dendrimer-modified GNRs conjugated with arginine-glycine-aspartic acid (RGD) peptide, which binds integrin  $\alpha_v \beta_3$  overexpressed on tumor vasculatures. They further observed the disappearance of tumors after iv injection of RGD-GNRs and NIR laser irradiation (808 nm, 24 W/cm<sup>2</sup>, 5 min).<sup>32</sup> However, numerous studies have revealed that monotherapy (e.g., chemotherapy, photothermal therapy, surgery, and other therapeutics) is not as effective as expected, which is attributed to individual differences in cancer patients, development of drug resistance, complicacy of the tumors and so on. The combination of photothermal therapy with other therapeutic strategies, especially chemotherapy, has shown promising prospect in recent years. 33,34 Here, we present a smart delivery platform with targeting and tunable release kinetics of DOX by capping polyelectrolyte layer by layer on GNRs to achieve synergistic chemo- and photo-thermal therapy, which facilitate the more precise temporal regulation of the dosing of bioactive molecules to the tumor. Several recent studies have utilized thermosensitive polymers decorated GNCs or GNRs for drug loading. Zhong et al. prepared GNRs-cored biodegradable micelles by coating GNRs

with lipoylated poly(ethylene glycol)-b-poly(ε-caprolactone) block copolymer and investigated for remotely triggered release of DOX and effective inhibition of drug-sensitive and multidrug-resistant (MDR) cancer cells. <sup>35</sup> Li and his co-workers designed PEGylated PAMAM dendrimer-doxorubicin conjugate-hybridized gold nanorod for synergistic hyperthermia ablation and chemotherapy. <sup>36</sup> However, a burst release of the loaded drugs was all observed in these studies when the nanocarriers were exposed to NIR light, due to the photothermal phase transition of the coating polymer. In this study, the LbL assembly technique was introduced, ideally achieving release of the compounds to the interest site due to gradual surface erosion by the introduction of NIR light irradiation. Meanwhile, the hyperthermia produced by the GNRs irradiated by the light, which further contributed to the favorable tumor therapy effect. This strategy, emphasizing on the synergistic therapy effect and the controlled release of active molecules, provides a valuable reference for combined tumor therapy studies in preclinical and clinical.

#### 4. Conclusions

In summary, we have developed a GNR and DOX-encapsulated microcapsule system for combined thermal therapy and chemotherapy *in vivo*. The microcapsules, which had a diameter of 2.6±0.4 µm, possessed a high drug-loading capacity. The breakdown of the microcapsule was triggered by NIR irradiation, allowing controlled release of the entrapped drug to target tissues. The microcapsules were shown to have low biotoxicity effects on cells and tissues and their tumor-targeting capabilities were substantially improved by conjugating a specific ligand (FA) to their surface. The

therapeutic effect and tumor inhibition of FA-MC@GNRs/DOX with NIR irradiation was more pronounced than free DOX or GNRs+laser. Our results indicate that FA-MC@GNRs/DOX is a promising design strategy for tumor-targeted imaging as well as synergistic combined therapy.

# Acknowledgments

The authors are grateful to Natural Science Foundation Committee of China (NSFC 81220108012, 61335007, 81371684and 81171395) and a project funded by the Priority Academic Program Development of Jiangsu Higher Education Institutions for their financial support.

# References

- 1 S. She, Q. Li, B. Shan, W. Tong and C. Gao, Adv. Mater., 2013, 25, 5814-5818.
- 2 B. V. Parakhonskiy, A. M. Yashchenok, M. Konrad and A. G. Skirtach, *Adv. Colloid. Interface. Sci.*, 2014, **207**, 253-256.
- 3 C. S. Karamitros, A. M. Yashchenok, H. Möhwald, A. G. Skirtach and M. Konrad, *Biomacromolecules.*, 2013, **14**, 4398-4406.
- 4 J. Huang, Q. Shu, L. Wang, H. Wu, A. Y. Wang and H. Mao, *Biomaterials.*, 2015, 39, 105-113.
- 5 Y. H. Roh, J. B. Lee, K. E. Shopsowitz, E. C. Dreaden, S. W. Morton, Z. Poon, J. Hong, I. Yamin, D. K. Bonner and P. T. Hammond, *ACS. Nano.*, 2014, **8**, 9767-9780.
- 6 T. Boudou, P. Kharkar, J. Jing, R. Guillot, I. Pignot-Paintrand, R. Auzely-Velty and C. Picart, J. Control. Release., 2012, 159, 403-412.
- 7 Y. Chen, D. Ye, M. Wu, H. Chen, L. Zhang, J. Shi and L.Wang, Adv. Mater., 2014, 26, 7018-7025.
- 8 H. C. Yen, H. Cabral, P. Mi, K. Toh, Y. Matsumoto, X. Liu, H. Koori, A. Kim, K. Miyazaki, Y. Miura, N. Nishiyama and K. Kataoka, *ACS. Nano.*, 2014, **8**, 11591-11602
- P. K. Mandapalli, S. Labala, D. Vanamala, M. P. Koranglekar, L. A. Sakimalla and V.
   V. Venuganti, *Drug. Deliv.*, 2013, 21, 605-614.
- 10 L. Xiang and B. Amit, *J.Am. Chem. Soc.* 2009, **131**, 5718-5719.
- 11 G. De, J. K. Ko, T. Tan, H. Zhu, H. Li and J. Ma, Oncotarget., 2014, 5, 7734-7747.

- 12 H. Chen, B. Li, X. Ren, S. Li Y. Ma, S. Cui and Y. Gu, *Biomaterials.*, 2012, **33**, 8461-8476.
- 13 A. P. Johnston, M. M. Kamphuis, G. K. Such, A. M. Scott, E. C. Nice, J. K. Heath and F. Caruso, ACS. Nano., 2012, 6, 6667-6674.
- 14 H. Y. Chen, X. Zhang, S. H. Dai, Y. X. Ma, S. S. Cui, S. Achilefu and Y. Q. Gu, Theranostics., 2013, 3, 633-649.
- 15 Y. Mi, X. Liu, J. Zhao, J. Ding and S.S. Feng, *Biomaterials.*, 2012, 33, 7519-7529.
- 16 Q. Zhao, B. Han, Z. Wang, C. Gao, C. Peng and J. Shen, *Nanomed. Nanotechnol.*, 2007, 3, 63-74.
- 17 H. J. Shen, H. Shi, K. Ma, M. Xie, L. L. Tang, S. Shen, B. Li, X. S. Wang and Y. Jin, *Acta. Biomater.*, 2013, 9, 6123-6133.
- 18 S. De Koker, B. G. De Geest, C. Cuvelier, L. Ferdinande, W. Deckers, W. E. Hennink, S. C. De Smedt and N. Mertens, Adv. Funct. Mater., 2007, 17, 3754-3763.
- 19 X. Sun, X. Huang, X. Yan, Y. Wang, J. Guo, O. Jacobson, D. Liu, L. P. Szajek, W. Zhu, G. Niu, D. O. Kiesewetter, S. Sun and X. Chen, ACS. Nano., 2014, 8, 8438-8446.
- 20 W. S. Kuo, C. N. Chang, Y. T. Chang, M. H. Yang, Y. H. Chien, S. J. Chen, C. S. Yeh, *Angew. Chem. Int. Ed.*, 2010, 122, 2711-2715.
- 21 S. Hwang, J. Nam, S. Jung, J. Song, H. Doh and S. Kim, *Nanomedicine (Lond).*, 2014, **9**, 2003-2022.
- 22 W. I. Choi, K. Ja-Young, C. Kang, C. C. Byeon, Y. H. Kim and G. Tae, ACS. Nano.,

- 2011, **5**, 1995-2003.
- 23 C.J. Johnson, E. Dujardin, S.A. Davis, C.J. Murphy and S. Mann, *J. Mater. Chem.*, 2002, **12**, 1765-1770.
- 24 D. Volodkin, Adv. Colloid. Interface. Sci., 2014, 207, 306-324.
- 25 H. Chen, S. Li, B. Li, X. Ren, S. Li, D. M. Mahounga, S. Cui, Y. Gu and S. Achilefu, *Nanoscale.*, 2012, 4, 6050-6064.
- 26 A.G. Skirtach, A. A. Antipov and D. G. Shchukin, Langmuir., 2004, 20, 6988-6992.
- 27 J. L. Li, D. Day and M. Gu, Adv. Mater., 2008, **20**, 3866-3871.
- 28 O. Kreft, A.G. Skirtach, G. B. Sukhorukov and H. Möhwald, *Adv. Mater.*, 2007, **19**, 3142-3145.
- 29 K. Ariga, Y. M. Lvov, K. Kawakami, Q. Ji and J. P. Hill, Adv. Drug. Deliv. Rev., 2011, 63, 762-771.
- 30 V. R. Muzykantov, Expert. Opin. Drug. Deliv., 2010, 7, 403-427.
- 31 E. B. Dickerson, E. C. Dreaden, X. Huang, I. H. El-Sayed, H. Chu, S. Pushpanketh, J. F. McDonald and M. A. El-Sayed, *Cancer. Lett.*, 2008, **269**, 57-66.
- 32 Z. Li, P. Huang, X. Zhang, J. Lin, S. Yang, B. Liu, F. Gao, P. Xi, Q. Ren and D. Cui, Mol. Pharmaceutics, 2010, 7, 94-104.
- 33 S. Sherlock and H. Dai, *Nano. Res.*, 2011, **4**, 1248-1260.
- 34 Y. Matsushita-Ishiodori and T. Ohtsuki, Acc. Chem. Res., 2012, 45, 1039-1047.
- 35 Y. Zhong, C. Wang, L. Cheng, F. Meng, Z. Zhong and Z. Liu, Biomacromolecules., 2013, 14, 2411-2419.
- 36 X. Li, M. Takashima, E. Yuba, A. Harada and K. Kono, Biomaterials., 2014,

**35,** 6576-6584.

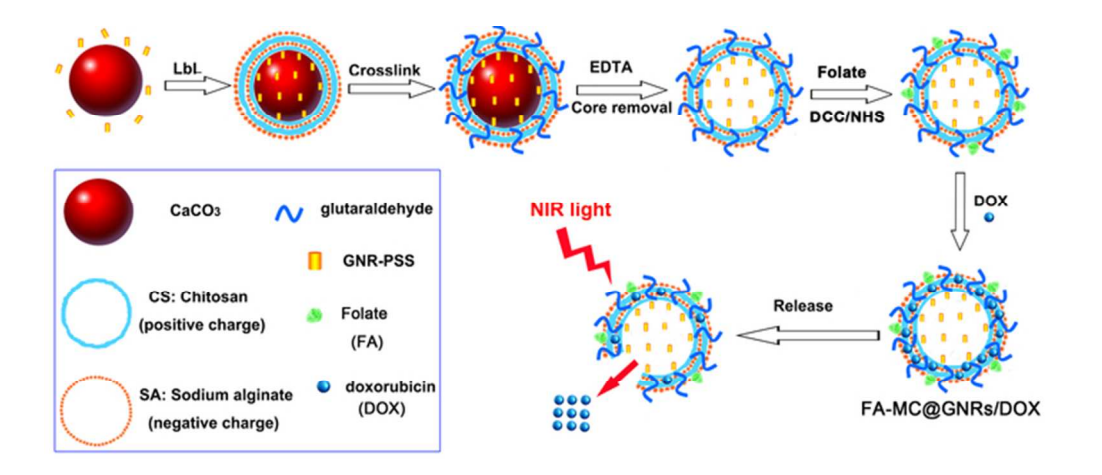


Figure 1: The synthesis routine of the multi-functional microcapsules (FA-MC@GNRs/DOX). 59x26mm (300 x 300 DPI)

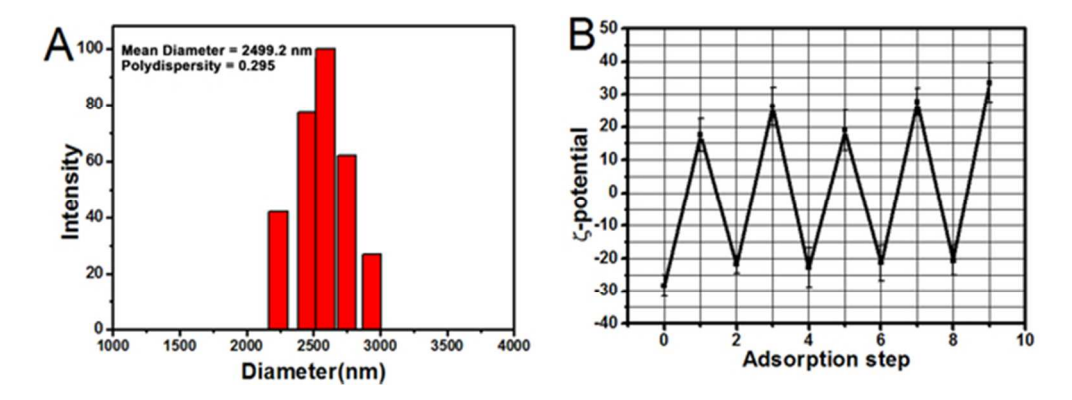


Figure 2: (A) The hydrodynamic diameter and polydispersity of MC@GNRs; (B) the different zeta-potential of MC@GNRs during its layer coating process. 51x19mm (300 x 300 DPI)

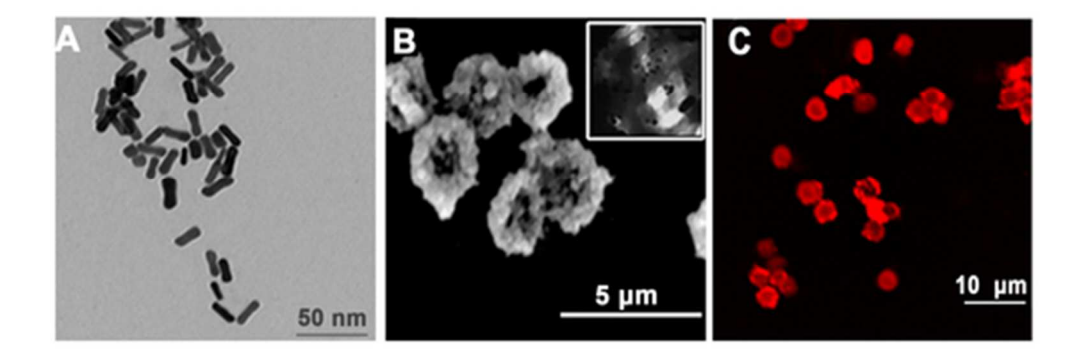


Figure 3: (A) TEM image of gold nanorods; (B) SEM image of FA-MC@GNRs/DOX; inserted: TEM image of FA-MC@GNRs/DOX; (C) laser confocal fluorescence image of FA-MC@GNRs/DOX.
41x14mm (300 x 300 DPI)

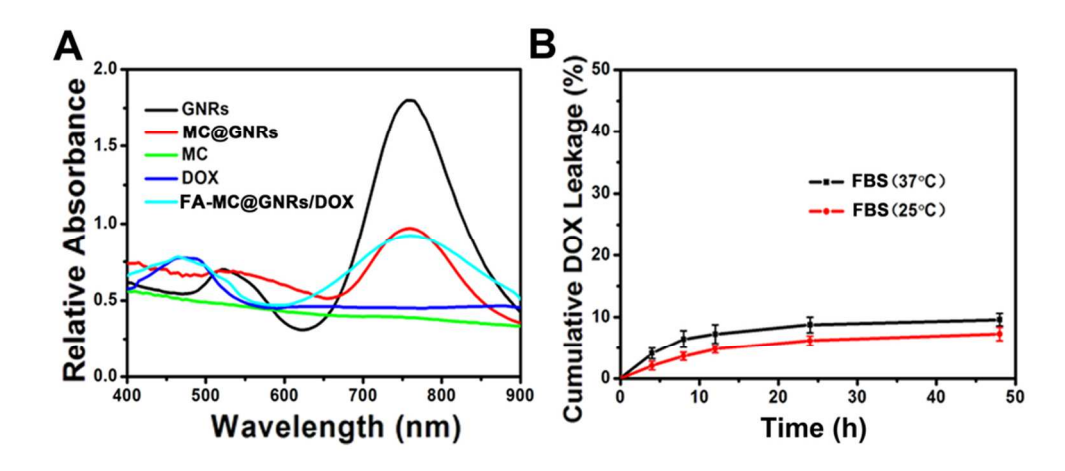


Figure 4: Absorption spectra of GNRs, MC, MC@GNRs, DOX and FA-MC@GNRs/DOX; (B) the DOX release profile in the presence of different incubation conditions (10 % FBS solution, 25 °C or 37 °C).

42x18mm (600 x 600 DPI)

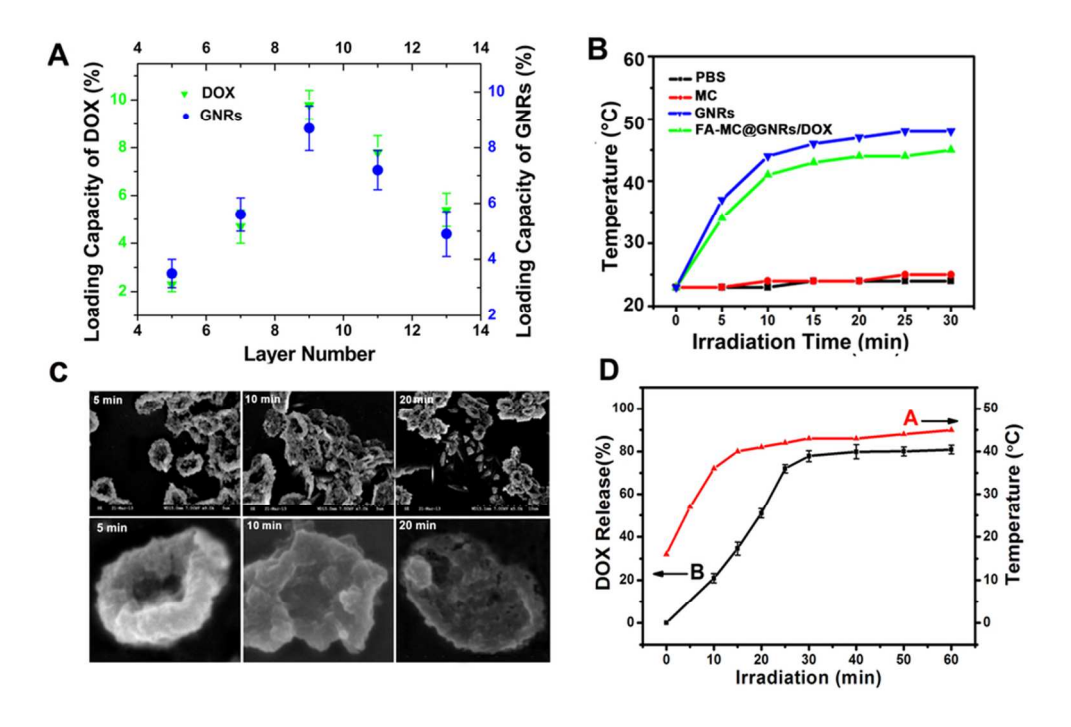


Figure 5: (A) Variation of the drug (DOX/GNRs) loading capacity as a function of the number of polyelectrolyte layers; (B) Temperature profile of PBS, MC, GNRs and FA-MC@GNRs/DOX under 765 nm laser irradiation; (C) morphology evolution of FA-MC@GNRs/DOX after NIR irradiation at 5 min, 10 min and 20 min; (D) release profile of DOX from FA-MC@GNRs/DOX (black) and the temperature increase of FA-MC@GNRs/DOX (red) in response to NIR irradiation.

81x54mm (300 x 300 DPI)

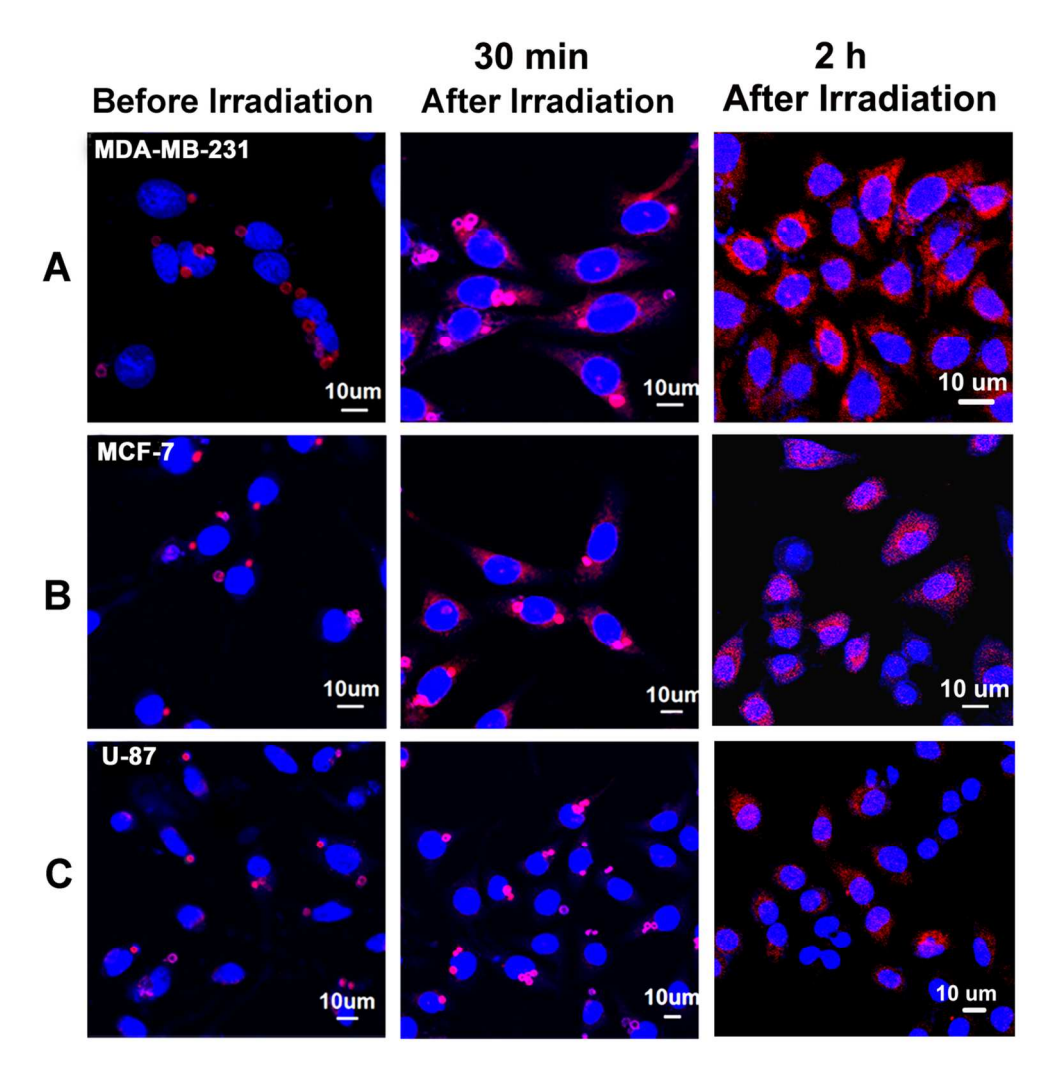


Figure 6: LCFM images of FA MC@GNRs/DOX incubated with (A) MDA-MB-231 cells, (B) MCF-7 cells and (C) U87 cells before and after laser (765 nm) irradiation. 117x119mm (300 x 300 DPI)

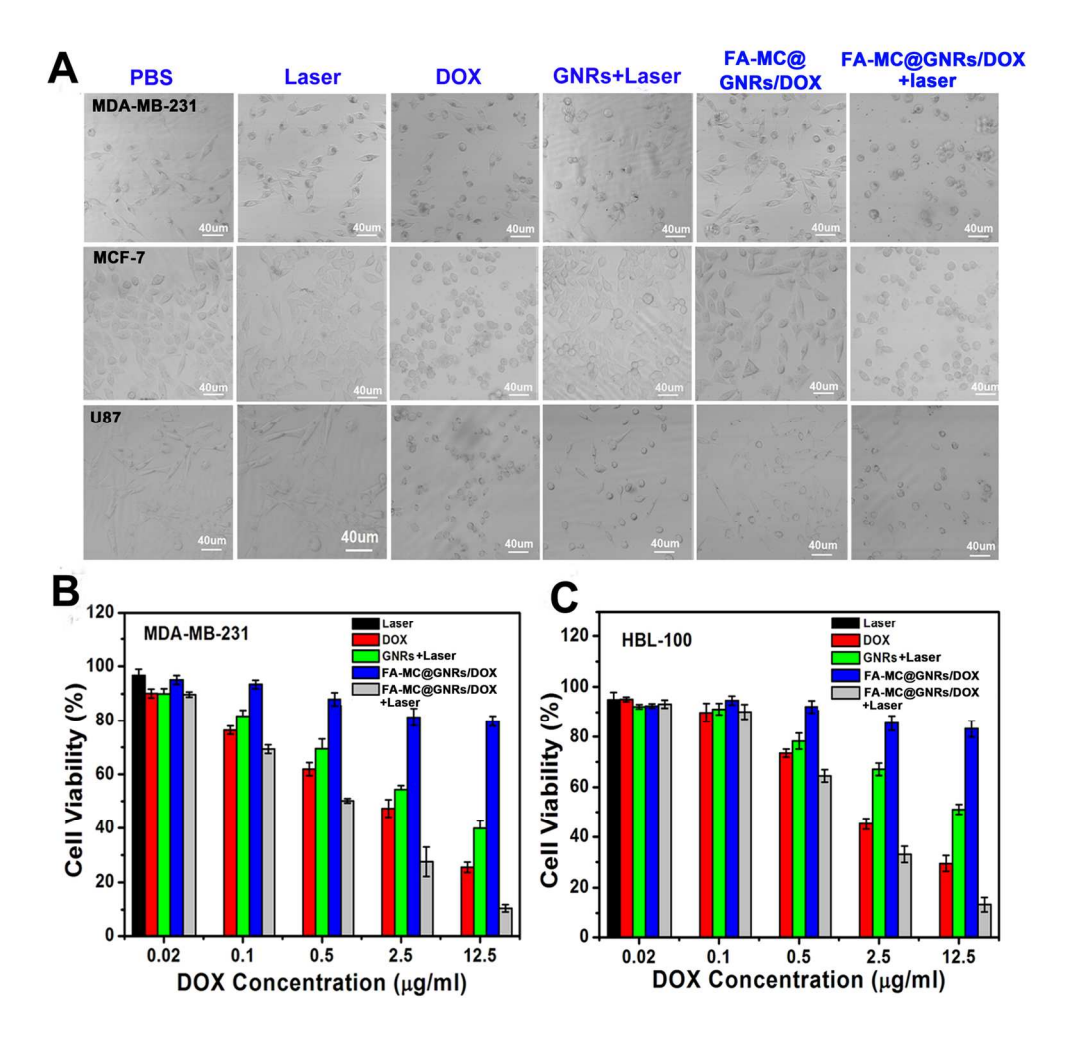


Figure 7: (A) The number and morphological change of MDA-MB-231 cells, MCF-7 cells and U87 cells after the six different treatments (PBS, laser, DOX, GNRs, FA-MC@GNRs/DOX and FA-MC@GNRs/DOX+laser) indicated by the DIC mode of LCFM; quantitative cytotoxic evaluation of different treatments (laser, DOX, GNRs+laser, FA-MC@GNRs/DOX and FA-MC@GNRs/DOX+laser) on (B) MDA-MB-231 cells and (C) HBL-100 cells by MTT assay.

149x148mm (300 x 300 DPI)

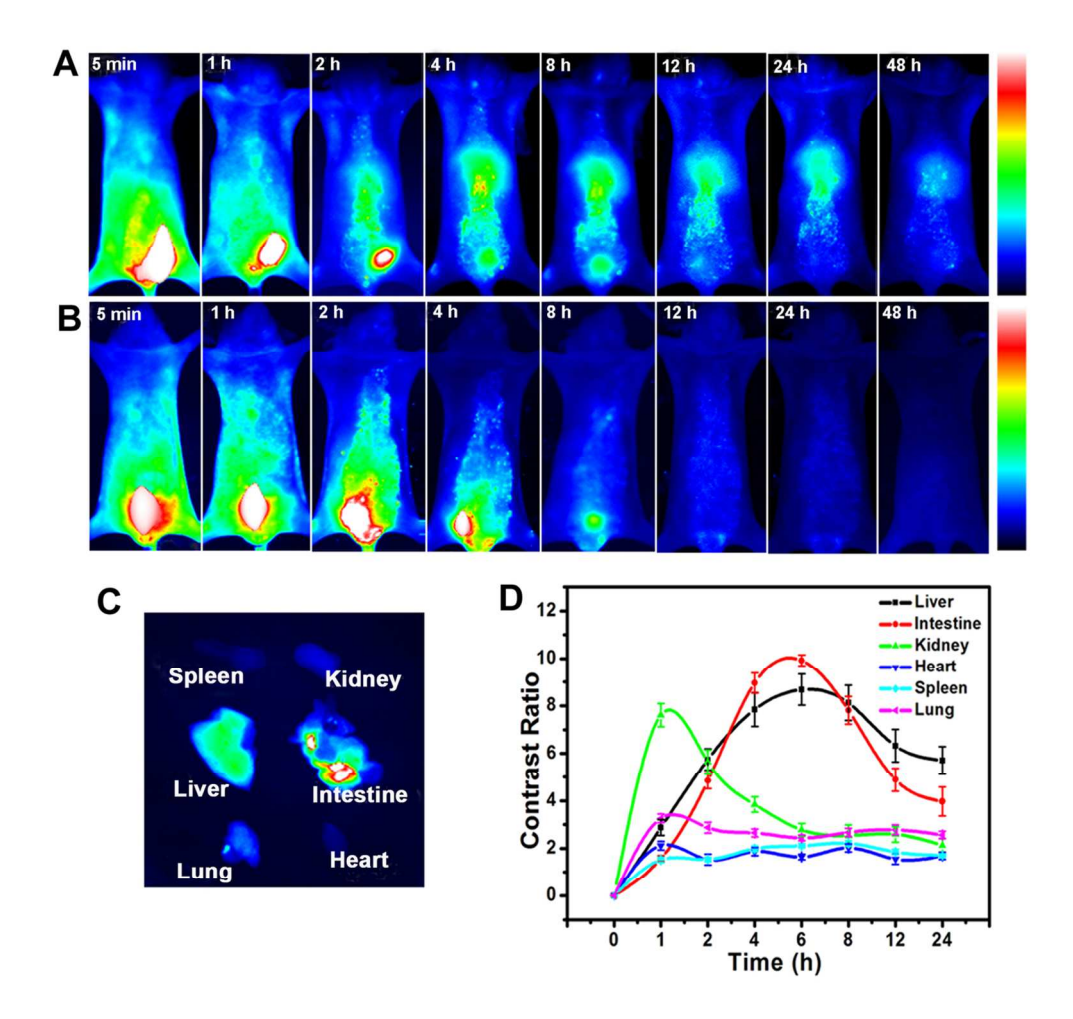


Figure 8: In vivo fluorescence imaging displaying the biodistribution of (A) FA-MC@GNRs/MPA and (B) MPA in normal mice at different post-injection time; (C) ex vivo fluorescence imaging of the main tissues (heart, liver, spleen, lung and kidney) obtained from normal mice after 24 h post-injection of FA-MC@GNRs/MPA; (D) the contrast ratios of different organs (heart, liver, spleen, lung and kidney) at different times examined analyzed by ROI semi-quantified analysis.

113x107mm (300 x 300 DPI)

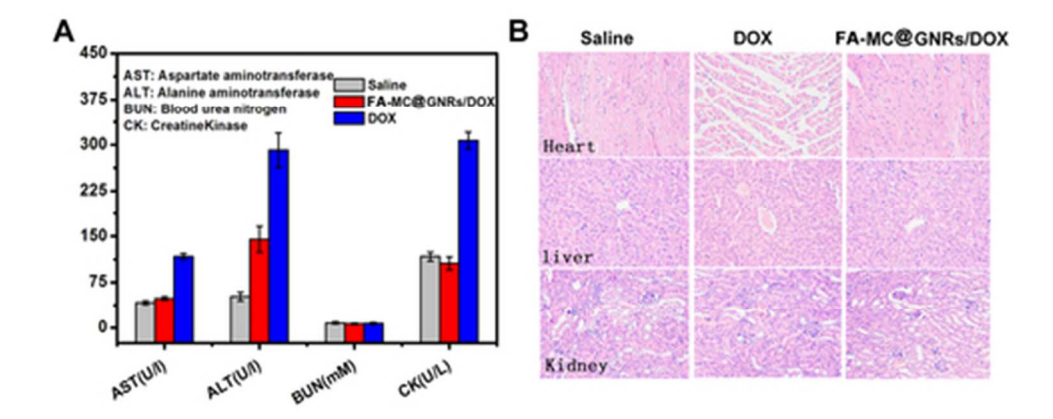


Figure 9: (A) The acute toxicities of saline, DOX, and FA-MC@GNRs/DOX on the mice was compared based on biochemical parameters, including ALT, AST, BUN, and CK; (B) histopathological analysis of the major organs (heart, liver and kidney) after different treatments(saline, DOX, and FA-MC@GNRs/DOX).

40x17mm (300 x 300 DPI)

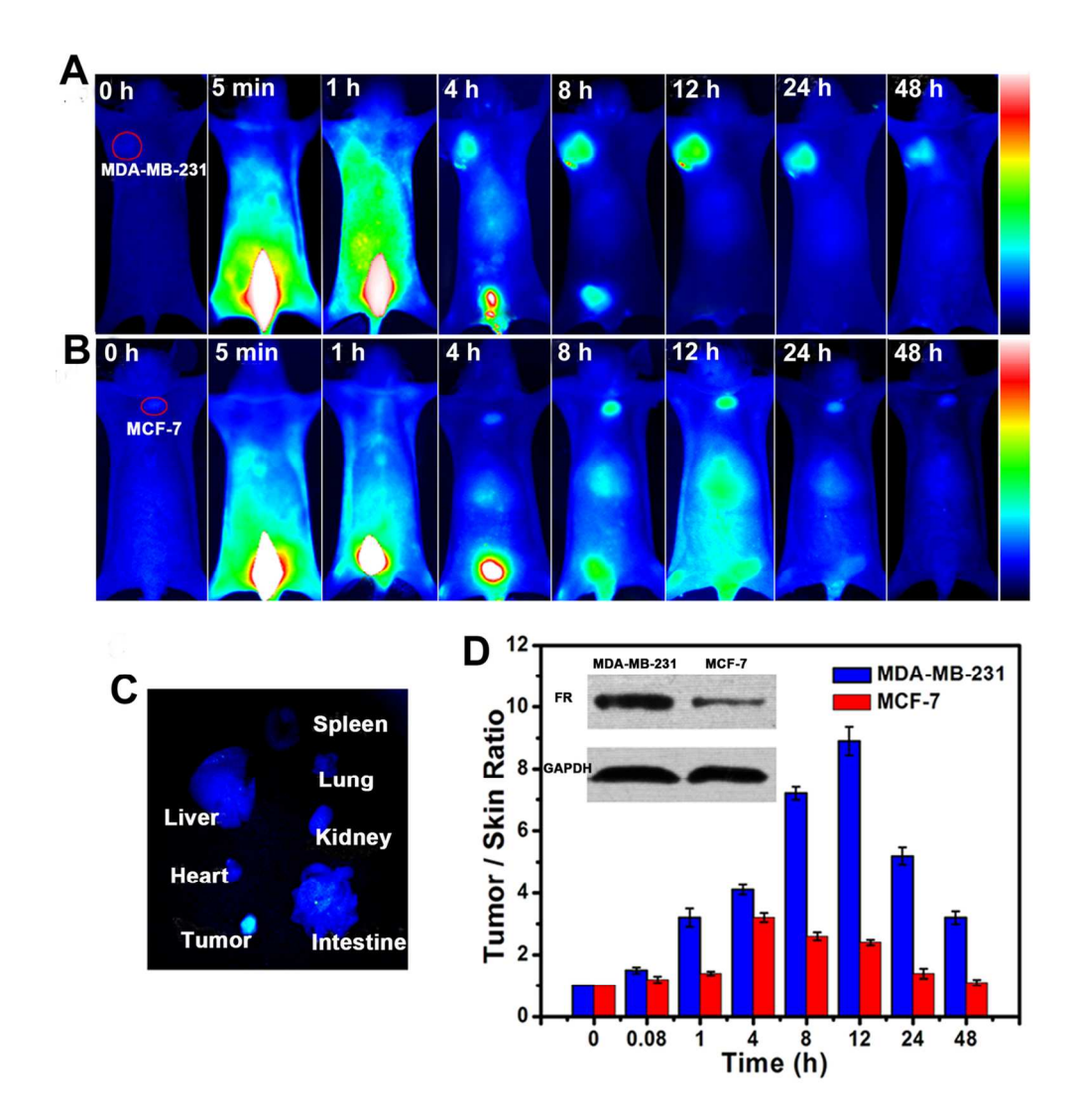


Figure 10: In vivo fluorescence images of FA-MC@GNRs/MPA in (A) MDA-MB-231 (high FR expression) and (B) MCF-7 (low FR receptor expression) in tumor-bearing mice at different times (5 min, 1 h, 4 h, 8 h, 12 h, 24 h and48 h); C) ex vivo fluorescence images of the isolated tissues(heart, liver, spleen, lung, kidney, intestine, and tumor) from MDA-MB-231 tumor-bearing mice at 48h post-injection; D) tumor-to-normal tissue (T/N) ratios of FA-MC@GNRs/MPA in MDA-MB-231 and MCF-7 mice at different post-injection times; Insert: FA receptor expression levels of MDA-MB-231 and MCF-7 cells.

124x129mm (300 x 300 DPI)

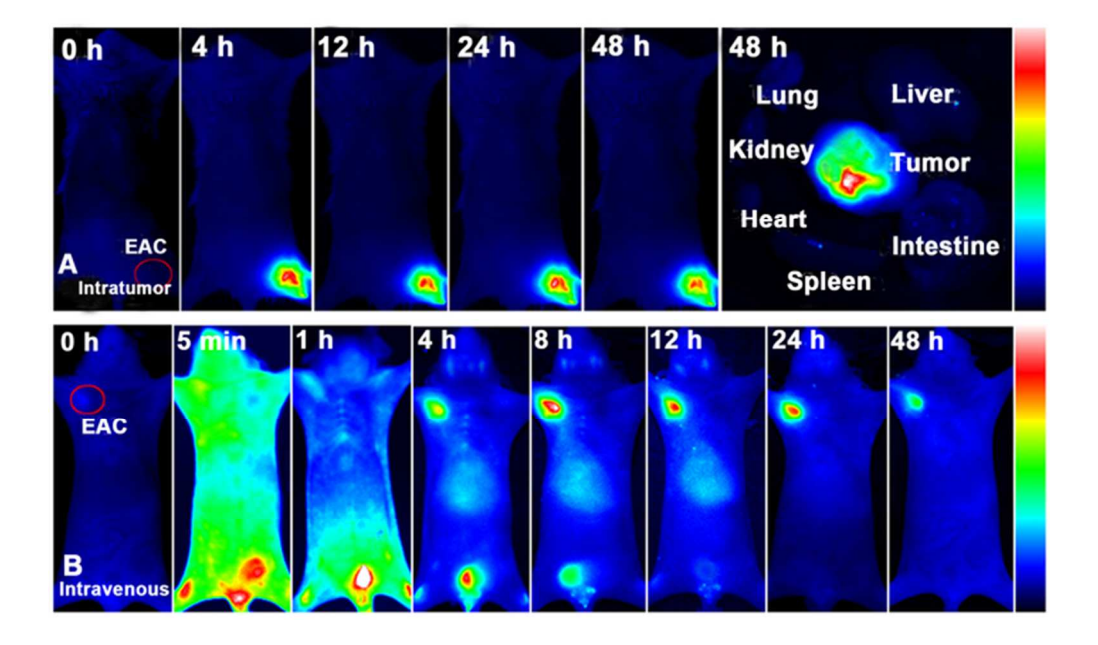


Figure 11: Fluorescence images displaying both (A) intratumoral and (B) intravenous injection of FA-MC@GNRs/MPA in EAC (high FR level) tumor-bearing miceover48 h. The ex vivo fluorescence images of isolated tissues (heart, liver, spleen, lung, kidney, intestine, and tumor) were obtained from the EAC tumor-bearing mice 48h post-intratumoral injection.

59x35mm (300 x 300 DPI)

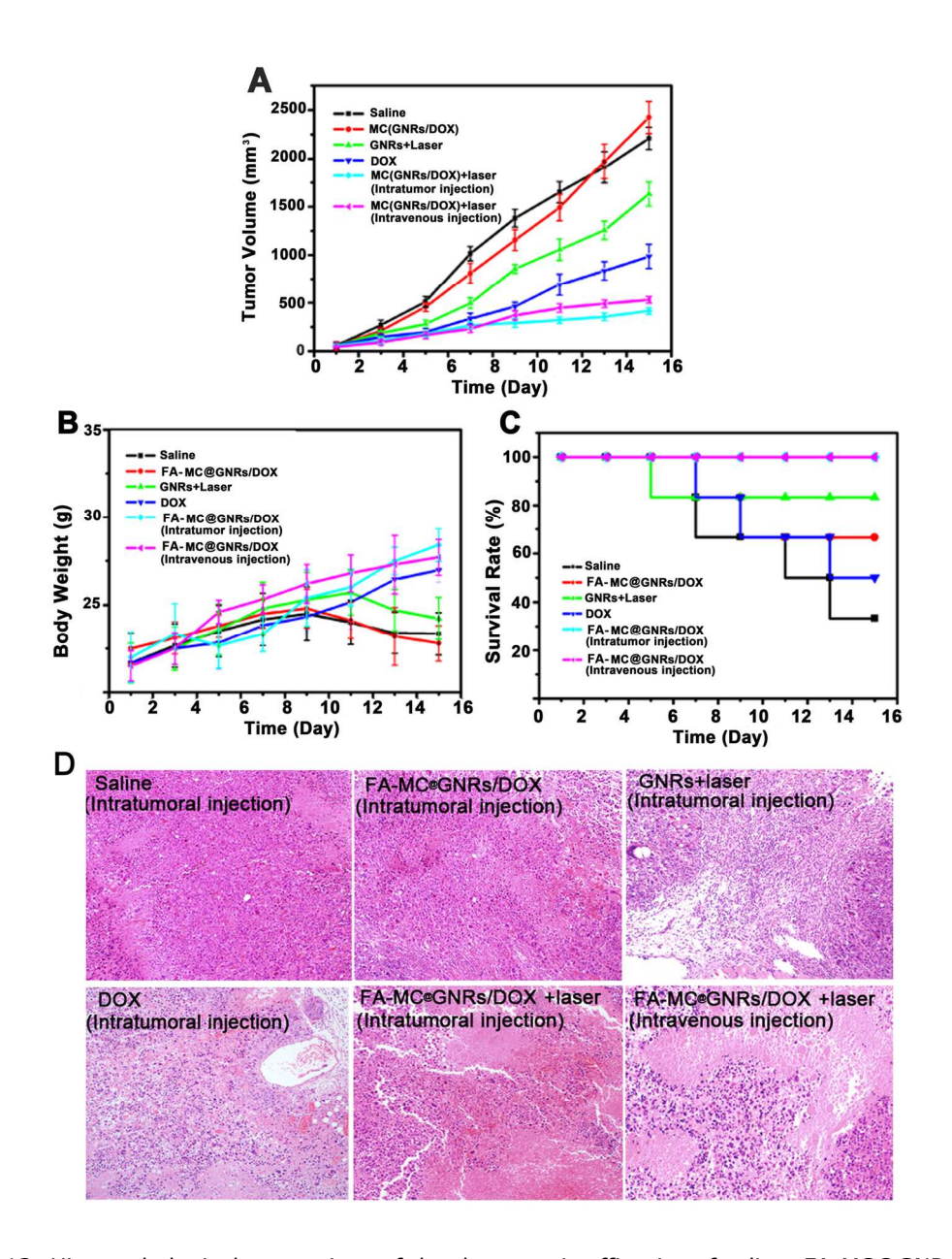


Figure 12: Histopathological comparison of the therapeutic efficacies of saline, FA-MC@GNRs/DOX, GNRs+laser, DOX, FA-MC@GNRs/DOX (intratumoral) + laser, and FA-MC@GNRs/DOX (intraveous) + laser in EAC tumor-bearing mice. (A) Tumor growth in mice by treatment group; (B) mice weight changes over 15 days by treatment group; (C) survival rates of mice over15 days by treatment group; (D) H&E-stained tumor tissue of the treated mice 15 days post-injection.

133x179mm (300 x 300 DPI)